International Journal of Decision Science
VOLUME 9 • NUMBER 1 • JUNE 2018

Sparse Nonrigid Registration of Point Sets Based on Thin Plate Spline

Pengpeng Zhang[a], Jie Yang [b] and Yuemin Zhu[c]
[a] *Shanghai Dianji University, School of Electronic and Information Engineering, Shanghai, China*
[b] *Shanghai Jiao Tong University, Institute of Image Processing and Pattern Recognition, Key Laboratory of System Control and Information Processing, Ministry of Education, Shanghai, China*
[c] *CNRS UMR5220, CREATIS; Inserm U1044; INSA Lyon; University of Lyon, France*
Corresponding author E-mail: zhangpp@sdju.edu.cn

ABSTRACT

Nonrigid registration of point sets is a common problem in many applications. Existing methods are highly sensitive to outliers because of l_2 norm. In this paper, a sparse nonrigid registration based on thin plate spline (SNR-TPS) for point sets is proposed. The method introduces *p*-norms in the measurement of error residuals to reduce the penalty for large outliers. A matching probability matrix is applied to construct the soft correspondence. Then TPS-based transformations are achieved using a combination of deterministic annealing and alternating direction method of multipliers (ADMM). The results on synthetic and real data show that the proposed SNR-TPS method outperforms the state-of-art methods when outliers are present in point sets.

Keywords: nonrigid registration, sparse, *p*-norms, thin plate spline, TPS-RPM.

1. INTRODUCTION

Nonrigid registration of point sets is a fundamental task in many applications, such as motion tracking, 3D reconstruction, medical image analysis and shape matching. The aim of nonrigid registration is to find a spatial transformation that optimally maps one point set onto the other. Since the transformation is nonrigid and the correspondence is unknown, achieving an accurate mapping is not a trivial work. To deal with this problem, the energy function of nonrigid registration is usually divided into two terms: error residual term and regularization term. The error residual term reflects the similarity between the two sets. The regularization term controls the transformation to avoid over-fitting. Both of two terms can be expressed as a norm formulation.

Since decades, many methods have been proposed. Based on the norm formulation, nonrigid registration methods are divided into two categories. One category used the l_2 norm in the two terms. Thin plate spline based robust point matching (TPS-RPM) [1, 2] was a representative method. With the soft correspondence and TPS-based transformations, TPS-RPM introduced the well-known iterative closet point (ICP) [3] method into nonrigid registration. The outliers were controlled by a weighting function. Some other researchers attempted to get the optimal solution by pruning the outliers. A representative pruning method was random sample consensus (RANSAC)[4]. Because of the randomness of sampling, RANSAC usually falls into local minimum. Optimal RANSAC [5] integrated many local RANSAC methods [6–8] to a unique reproducible method to get the optimal solution. In contrast to these methods, coherent point drift (CPD) [9, 10] method represented the nonrigid registration as a mixture density estimation problem. Two point sets were treated as a Gaussian mixture model (GMM) centroid set and a sample point set from this GMM, respectively. The outliers were controlled by a fixed value of outliers ratio. To define the outliers ratio automatically, several variants [11–13] were proposed. The survey of nonrigid registrations [14] analyzed the registration of 3D point sets from the view point of data fitting. Although these methods are more or less effective for some applications, the optimization in all of them used a least-squares formulation. This implies a basic assumption that error residuals are normal, which is highly sensitive to outliers.

Instead of weighting or pruning outliers, the sparsity of error residuals was introduced to handle outliers. Many methods used l_1 norm to model inliers or outliers, such as nonrigid ICP with statistical shape model (NICP-SSM) [15] and sparse deformable model with l_1 norm regularization (SDM-l_1)[16]. In these methods, the shape model was an important part in achieving accurate transformation. Recently, a sparse nonrigid registration (SNR)[17] was proposed. The transformation was estimated based on the '1 regularization term when the deformable object is piecewise smooth. Though the shape model was not used in the SNR method, the accuracy of registration was highly dependent on the initial correspondence. Besides, SNR requires knowledge not only about the location of points but also about the relationship between the points to get accurate results.

Since *p*-norms ($p \in [0,1]$) outperform l_1 norm in inducing sparsity [18], they have been applied in rigid registration. Sparse ICP (SICP) [19] and its variant ESICP [20] were two representative methods. Though SICP and ESICP effectively handled outliers in rigid registration, they failed when directly applied to nonrigid registration. They were usually used as an initial registration method, then another nonrigid registration method, e.g. TPS-RPM, was used to achieve final nonrigid transformation. Using these methods, sparsity cannot be effective for nonrigid registration. In this paper, we propose a sparse nonrigid registration method based on thin plate spline (SNR-TPS). Sparsity is directly applied to nonrigid registration. Our method introduces *p*-norms ($p \in [0,1]$) in the error residual term to handle outliers, uses alternately soft correspondence and TPS to estimate the correspondence and transformations, and optimizes energy function by a combination of deterministic annealing and alternating direction method of multipliers (ADMM) [21].

The rest of the paper is organized as follows. After presenting the principle of thin plate spline based robust point matching (TPS-RPM) in Section 2, the proposed SNR-TPS method is described in Section 3. The results on synthetic data and real data from cranio-maxillofacial surgery planning are presented in Section 4, followed by conclusion in Section 5.

2. PRINCIPLE OF THIN PLATE SPLINE BASED ROBUST POINT MATCHING

Given a data set $\mathbf{X} = \{\mathbf{x}_1, \mathbf{x}_2, \ldots, \mathbf{x}_{Nx}\}$ and a model set $\mathbf{Y} = \{\mathbf{y}_1, \mathbf{y}_2, \ldots, \mathbf{y}_{Ny}\}$, the task is to estimate a nonrigid transformation which effectively maps the data set onto the model set. Due to the coupled problem of unknown correspondence and transformation, an iterative method is usually applied for nonrigid registration.

TPS-RPM [1, 2] is a popular iterative method for nonrigid registration of point sets. To deal with outliers, soft correspondence is built by a matching probability matrix **M**. Then TPS is applied to model the nonrigid registration. In this framework, the nonrigid transformation is divided into an affine transformation **d** and a non-affine warping coefficient matrix **w** of TPS. The associated energy function is given by:

$$
\begin{aligned}
&E(\mathbf{M},\mathbf{d},\mathbf{w}) = \sum_{i=1}^{Nx}\sum_{j=1}^{Ny} m_{ij} \left\| \mathbf{x}_i\mathbf{d} + \phi(\mathbf{x}_i)\mathbf{w} - \mathbf{y}_j \right\|_2^2 \\
&-\varsigma \sum_{i=1}^{Nx}\sum_{j=1}^{Ny} m_{ij} + T\sum_{i=1}^{Nx}\sum_{j=1}^{Ny} m_{ij}\left(\log m_{ij} - 1\right) \\
&+\lambda_1 tr\left(\mathbf{w}^T \Phi \mathbf{w}\right) + \lambda_2 tr\left(\left(\mathbf{d}-\mathbf{I}\right)^T\left(\mathbf{d}-\mathbf{I}\right)\right) \\
&s.t. \\
&\sum_{i=1}^{Nx+1} m_{ij} = 1,\ j = 1,2,\cdots,Ny \\
&\sum_{i=1}^{Ny+1} m_{ij} = 1, i = 1,2,\cdots,Nx
\end{aligned}
\tag{1}
$$

The first term is error residual term. $\phi(\mathbf{x}_i)$ is the kernel function of TPS, and $\Phi = \{\phi(\mathbf{x}_1), \phi(\mathbf{x}_2), \cdots, \phi(\mathbf{x}_{Nx})\}$. The minimization of this term aims to deform each $\mathbf{x}_i$ to its counterpart $\mathbf{y}_j$. The second and third terms are used to ensure $m_{ij} \in [0,1]$. T is the temperature parameter of

deterministic annealing algorithm. The fourth term is a regularization term to punish non-affine local warping coefficient **w**. The fifth term is used to avoid unphysical reflection transformation of **d**. ς, λ_1, and λ_2 are regularization parameters. ς is usually set to a value close to zero. The values of λ_1 and λ_2 are linked to temperature *T*.

Though TPS-RPM somewhat controls outliers by soft correspondence, its final transformations will not be optimal when the error residual of an outlier is much larger than others. Besides, error residuals were still assumed to be a normal distribution when using the l_2 norm. However, this assumption will be substantially violated if there are outliers.

3. SPARSE NONRIGID REGISTRATION BASED ON THIN PLATE SPLINE

With respect to the existing TPS-RPM method, we propose so-called SNR-TPS method that consists of using *p*-norms ($p \in [0,1]$) to measure error residuals. The value of *p* controls the penalty of outliers. For a small value of *p*, large outliers will not induce large penalties (Fig. 1). This means that the optimization cannot be deviated when reducing the large penalty associated with an outlier. Figure 1 indicates that the performance of alignment is gradually improved by decreasing the value of *p*. The histograms demonstrate the sparse character of our method. As decreasing the value of *p*, more error residuals of the

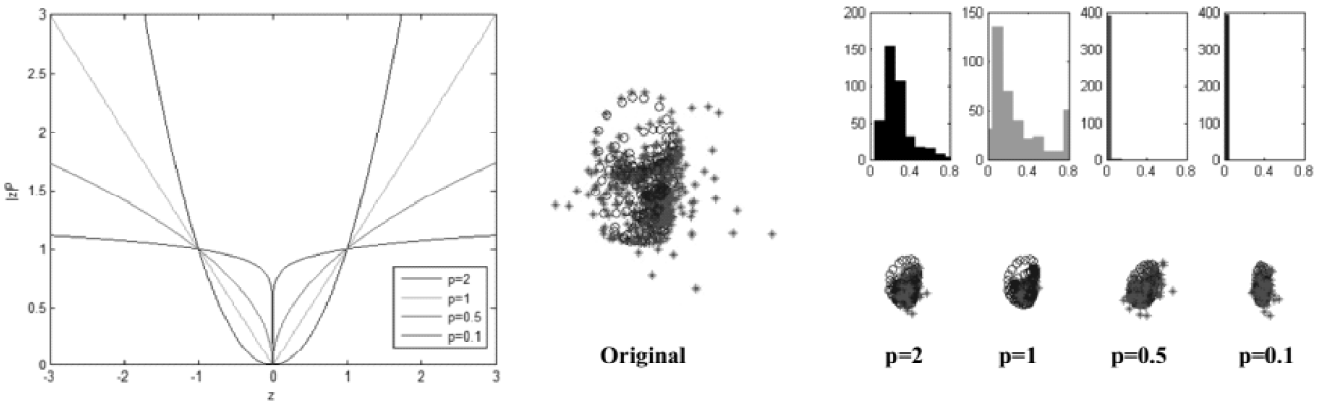

Figure 1: Left: behaviors of *p*-norms used to measure error residuals in our method. Right: alignment of 3D face[10] with different values of *p*.

counterparts equal zero, and the non-zero error residual is few. The sparsity of error residual term ensures the performance of nonrigid registration.

In contrast to TPS-RPM, *p*-norms are used in the proposed SNR-TPS method to measure error residuals. Hence, the energy function of the proposed SNR-TPS method can be formulated as:

$$
\begin{aligned}
E(\mathbf{M},\mathbf{d},\mathbf{w}) &= \sum_{i=1}^{Nx}\sum_{j=1}^{Ny} m_{ij}\left\|\mathbf{x}_i\mathbf{d}+\phi(\mathbf{x}_i)\mathbf{w}-\mathbf{y}_j\right\|_2^p \\
&-\varsigma\sum_{i=1}^{Nx}\sum_{j=1}^{Ny} m_{ij} + T\sum_{i=1}^{Nx}\sum_{j=1}^{Ny} m_{ij}\left(\log m_{ij}-1\right) \\
&+\lambda_1 tr\left(\mathbf{w}^T\Phi\mathbf{w}\right)+\lambda_2 tr\left((\mathbf{d}-\mathbf{I})^T(\mathbf{d}-\mathbf{I})\right)
\end{aligned}
$$

$$
\begin{aligned}
&s.t. \\
&\sum_{i=1}^{Nx+1} m_{ij} = 1,\ j=1,2,\cdots,Ny \\
&\sum_{i=1}^{Ny+1} m_{ij} = 1, i=1,2,\cdots,Nx
\end{aligned}
\qquad (2)
$$

where the error residual term is expressed as a function $\varphi(r)=|r|^p\ (p\in[0,1])$ and $r=\|\cdot\|_2$.

This energy function can be solved iteratively by a well-known two-step optimization:

Step 1. Estimation of soft correspondence:

$$
\begin{aligned}
&\arg\min_{\mathbf{M}} \sum_{i=1}^{Nx}\sum_{j=1}^{Ny} m_{ij}\left\|\mathbf{x}_i\mathbf{d}+\phi(\mathbf{x}_i)\mathbf{w}-\mathbf{y}_j\right\|_2^p \\
&-\varsigma\sum_{i=1}^{Nx}\sum_{j=1}^{Ny} m_{ij} + T\sum_{i=1}^{Nx}\sum_{j=1}^{Ny} m_{ij}\left(\log m_{ij}-1\right)
\end{aligned}
\qquad (3)
$$

Step 2. Estimation of affine transformation **d** and non-affine warping coefficient matrix **w** of TPS:

$$\begin{aligned}&\arg\min_{\mathbf{M}} \sum_{i=1}^{Nx}\sum_{j=1}^{Ny} m_{ij}\left\|\mathbf{x}_i\mathbf{d}+\phi\left(\mathbf{x}_i\right)\mathbf{w}-\mathbf{y}_j\right\|_2^p \\ &+\lambda_1 tr\left(\mathbf{w}^T\Phi\mathbf{w}\right)+\lambda_2 tr\left(\left(\mathbf{d}-\mathbf{I}\right)^T\left(\mathbf{d}-\mathbf{I}\right)\right)\end{aligned} \tag{4}$$

However, the above two problems are non-convex and non-smooth. To obtain a robust and efficient solution, deterministic annealing will be combined with ADMM [21] as explained later.

3.1. Estimation of soft correspondence

Since $\varphi(r)=|r|^p\ (p\in[0,1])$ is a non-decreasing function when $r=\|\cdot\|_2, \left\|\|\cdot\|_2\right|^p$ has the same minimum point as $\|\cdot\|_2$. Consequently, the optimization in Eq. 3 is equivalent to

$$\begin{aligned}&\arg\min_{\mathbf{M}} \sum_{i=1}^{Nx}\sum_{j=1}^{Ny} m_{ij}\left\|\mathbf{x}_i\mathbf{d}+\phi\left(\mathbf{x}_i\right)\mathbf{w}-\mathbf{y}_j\right\|_2^2 \\ &-\varsigma\sum_{i=1}^{Nx}\sum_{j=1}^{Ny} m_{ij}+T\sum_{i=1}^{Nx}\sum_{j=1}^{Ny} m_{ij}\left(\log m_{ij}-1\right)\end{aligned} \tag{5}$$

This optimization function is the same as that in the TPS-RPM method. Hence, the soft corresponding point of $\mathbf{x}_i$ can be attained as follows:

$$\mathbf{c}_i=\sum_{j=1}^{Ny} m_{ij}\mathbf{y}_j \Big/ \sum_{j=1}^{Ny} m_{ij} \tag{6}$$

where $m_{ij}=\exp\left(-\dfrac{\left\|\mathbf{x}_i\mathbf{d}+\phi\left(\mathbf{x}_i\right)\mathbf{w}-\mathbf{y}_j\right\|_2^2-\varsigma}{T}\right)$.

3.2. Estimation of transformation

We introduce a new set of error residual variables $\mathbf{Z}=\left\{\mathbf{z}_1,\mathbf{z}_2,\cdots,\mathbf{z}_{Nx}\right\}$ to optimize Eq. 4:

$$\begin{aligned}&\arg\min_{\mathbf{d},\mathbf{w},\mathbf{Z}} \sum_{i=1}^{Nx}\left\|\mathbf{z}_i\right\|_2^p+\lambda_1 tr\left(\mathbf{w}^T\Phi\mathbf{w}\right)+\lambda_2 tr\left(\left(\mathbf{d}-\mathbf{I}\right)^T\left(\mathbf{d}-\mathbf{I}\right)\right) \\ &s.t. \\ &\delta_i=0\end{aligned} \tag{7}$$

where $\delta_i=\mathbf{x}_i\mathbf{d}+\phi\left(\mathbf{x}_i\right)\mathbf{w}-\mathbf{c}_i-\mathbf{z}_i$.

The above equation is an optimization problem with one constraint. Augmented Lagrangian method (ALM) is an effective method to solve this problem. Hence, we define the associated ALM function of Eq. 7 as

$$\begin{aligned}&L\left(\mathbf{d},\mathbf{w},\mathbf{Z},\mathbf{A}\right)=\sum_{i=1}^{Nx}\left\|\mathbf{z}_i\right\|_2^p+\mathbf{a}_i^T\delta_i+\frac{\mu}{2}\left\|\delta_i\right\|_2^2 \\ &+\lambda_1 tr\left(\mathbf{w}^T\Phi\mathbf{w}\right)+\lambda_2 tr\left(\left(\mathbf{d}-\mathbf{I}\right)^T\left(\mathbf{d}-\mathbf{I}\right)\right)\end{aligned} \tag{8}$$

where $\mathbf{A}=\left\{\mathbf{a}_1,\mathbf{a}_2,\cdots,\mathbf{a}_{Nx}\right\}$ is a Lagrangian multipliers set, and $\mu>0$ is a penalty weight.

To minimize the above ALM function, ADMM[21] was adopted in the proposed method. The transformations are estimated in three steps:

Step 2.1. Estimation of error residual variable **Z**:

$$\arg\min_{\mathbf{Z}} \sum_{i=1}^{Nx}\left\|\mathbf{z}_i\right\|_2^p+\frac{\mu}{2}\left\|\mathbf{z}_i-\mathbf{h}_i\right\|_2^2 \tag{9}$$

Step 2.2. Estimation of TPS-based nonrigid transformations:

$$\begin{aligned}&\arg\min_{\mathbf{d},\mathbf{w}} \sum_{i=1}^{Nx}\left\|\mathbf{x}_i\mathbf{d}+\phi\left(\mathbf{x}_i\right)\mathbf{w}-\mathbf{e}_i\right\|_2^2 \\ &+\lambda_1 tr\left(\mathbf{w}^T\Phi\mathbf{w}\right)+\lambda_2 tr\left(\left(\mathbf{d}-\mathbf{I}\right)^T\left(\mathbf{d}-\mathbf{I}\right)\right)\end{aligned} \tag{10}$$

Step 2.3. Update of Lagrangian multiplier $\mathbf{a}_i$:

$$\mathbf{a}_i=\mathbf{a}_i+\mu\delta_i \tag{11}$$

where $\mathbf{e}_i=\mathbf{c}_i+\mathbf{z}_i-\mathbf{a}_i/\mu$ and $\mathbf{h}_i=\mathbf{x}_i\mathbf{d}+\phi\left(\mathbf{x}_i\right)\mathbf{w}-\mathbf{c}_i+\mathbf{a}_i/\mu$.

Since each element $\mathbf{z}_i$ of **Z** is independent in Step 2.1, it can be optimized independently. In other words, the estimation of error residual variable **Z** can be separated as:

$$\sum_{i=1}^{Nx}\min_{\mathbf{z}_i}\left\|\mathbf{z}_i\right\|_2^p+\frac{\mu}{2}\left\|\mathbf{z}_i-\mathbf{h}_i\right\|_2^2 \tag{12}$$

Then the individual element $\mathbf{z}_i$ can be solved efficiently using the following shrinkage operator [22]:

$$\mathbf{z}_i^*=\begin{cases}0, & if\ \left\|\mathbf{h}_i\right\|_2\le\tilde{h}_i \\ \beta\mathbf{h}_i, & f\ \left\|\mathbf{h}_i\right\|_2>\tilde{h}_i\end{cases} \tag{13}$$

where $\tilde{h}_i = \alpha_a + \frac{p}{\mu}\alpha_a^{p-1}$ and $\alpha_a = \left(\frac{2}{\mu}(1-p)\right)^{\frac{1}{2-p}}$. β is a value linked to p. After two or three iterations, it will converge by initializing $\beta_i^0 \in \left[\alpha_a \|h_i\|_2^{-1}, 1\right]$, and $\beta_i^{(k+1)}$ is equal to $1-\frac{p}{\mu}\|h_i\|_2^{p-2}\left(\beta_i^{(k)}\right)^{p-1}$ at each iteration.

Indeed, Eq. 13 can be seen as a classification function with the threshold $\tilde{h}_i$. All points will be separated as inliers or outliers based on their error residuals. When $p=0$, β will always be one. That is a binary classification: $\mathbf{z}_i$ is either 0 or itself. Eq. 10 in Step 2.2 is similar to that in TPS-RPM method. The difference between them is only in the computation of the corresponding point $\mathbf{e}_i$. Therefore, the same QR decomposition for TPS was used in the proposed method.

3.3. Estimation of the value of p

p is a control parameter of outliers in the proposed SNR-TPS method. When $p=0$, the minimization of error residuals is equivalent to minimizing the number of non-zero elements in the variable $\mathbf{Z}$. Figure 1 shows that as *p* tends to 1, a strong penalty will be applied to an outlier having $\|\mathbf{z}_i\|_2 \gg 0$. Since the process of registration is from global to local, a fixed value of *p* cannot express this procedure very well.

With the deterministic annealing, a data set $\mathbf{X}$ is mapped onto the soft correspondence set $\mathbf{C} = \{\mathbf{c}_1, \mathbf{c}_2, \ldots, \mathbf{c}_{Nx}\}$ at each temperature. At the beginning, points in the data set $\mathbf{X}$ are far from their counterparts. *p* is set to one to get a large penalty for an obvious outlier. Then the current *p* is decreased based on the emerging error residuals *err* according to:

$$p = \frac{mean(err)}{\max(err) - \min(err)} \tag{14}$$

where $err = \|\mathbf{C} - \mathbf{X}_t\|_2^2$, $\mathbf{X}_t$ designating the current deformed set of $\mathbf{X}$. $mean(err)$, $\max(err)$ and $\min(err)$ are the mean, maximum and minimum value of error residuals *err*, respectively.

Eq. 14 means that when the distribution of error residuals is uniform, *p* will become large. The value of *p* gradually decreases with the increase of the difference between error residuals. In other words, the value of *p* will become smaller if more outliers are detected in the process of registration. However, the alignment of two point sets with outliers will lead to over-fitting if *p* is directly computed using Eq. 14. To remedy this, a learning rate is used to update *p*:

$$p = p^{old} + \frac{1}{\alpha_t}\left(p^{new} - p^{old}\right) \tag{15}$$

where p^{new} is defined by Eq. 14, p^{old} is the old *p* at the last iteration, and α_t is the learning rate.

The learning rate α_t is an empirical parameter allowing to avoid over-learning. In the present study, α_t is an increasing value and set to the current iteration time t. At the initial iteration, p updates faster to get a rapid optimization. Then it updates more slowly to avoid over-fitting. The complete algorithm of the proposed SNR-TPS method is summarized below.

Algorithm 1 The proposed SNR-TPS method

Input: data set **X**, model set **Y**
1: Initialize: **M**, **d**, **w**, λ_1, λ_2, T, and p
2: **for** each temperature T **do**
3: Find soft correspondence using Eq. 6
4: **while** not converged **do**
5: Solve **Z** by Eq. 13
6: Solve **d** and **w** using QR decomposition for TPS
7: Update the value of p by Eqs. 14 and 15
8: Update Lagrangian multipliers set **A** by Eq. 11
9: **end while**
10: Decrease T, λ_1 and λ_2
11: **end for**
Output: **d**, **w**, and transformed data set $\mathbf{X}_t$,

Figure 2: Algorithm of SNR-TPS method

4. EXPERIMENTAL RESULTS

The performance of the proposed SNR-TPS method is evaluated by comparing it with some related nonrigid registration methods (TPS-RPM and SNR). Matching error is measured by Root Mean Square Error (RMSE). It is defined as $\sqrt{\frac{1}{N}\sum_{i=1}^{N}\left\|\mathbf{T}(\mathbf{x}_i)-\mathbf{c}_i\right\|_2^2}$, where $\mathbf{c}_i$ is the counterpart of $\mathbf{x}_i$, N is the number of corresponding points and $\mathbf{T}$ is the transformation matrix. When the ground-truth $\mathbf{g}_i$ is known, $\mathbf{c}_i$ is replaced by $\mathbf{g}_i$.

Throughout the paper, unless otherwise specified, an adaptive value of p was applied. To evaluate the sparsity in the different optimization terms, SNR [17] is implemented with correspondence by k-d tree and without multi-resolution. The comparative experiments were focused on two classes of outliers: noisy and incomplete datasets, which are the most challenging problems in nonrigid registration. Two simple but yet demonstrative examples of 3D face and 3D bunny [10] were used as the original datasets.

4.1. Results on noisy datasets

Random noise was proportionally added in the original 3D face and 3D bunny datasets.10 Noise ratios was set from 10% to 100% for 3D face, and set to 10%, 20% and 30% for 3D bunny. Two situations were considered: noisy data set and noisy model set.

Quantitative comparison and matching results are shown in Figs. 3 and 4. Our method performs better than the other methods for both noisy data set and noisy model set whatever the noise ratio is. The performance of our method is little affected by the noise in the model set.

The results indicate that our method more easily detects noise than the other methods. As we know, the use of soft correspondence can reduce, but cannot avoid the influence of noise. Therefore, TPS-RPM does not align two faces or bunnies well in case of noisy data or noisy model sets. TPS-RPM produces the worst alignments though its RMSE is not the worst. Due to the sparsity of the regularization term, over-fitting occurs when using SNR method. In the presence of noise, SNR transforms all points into model points, no matter it is a noisy point or a data point. For example, when noise is present in the

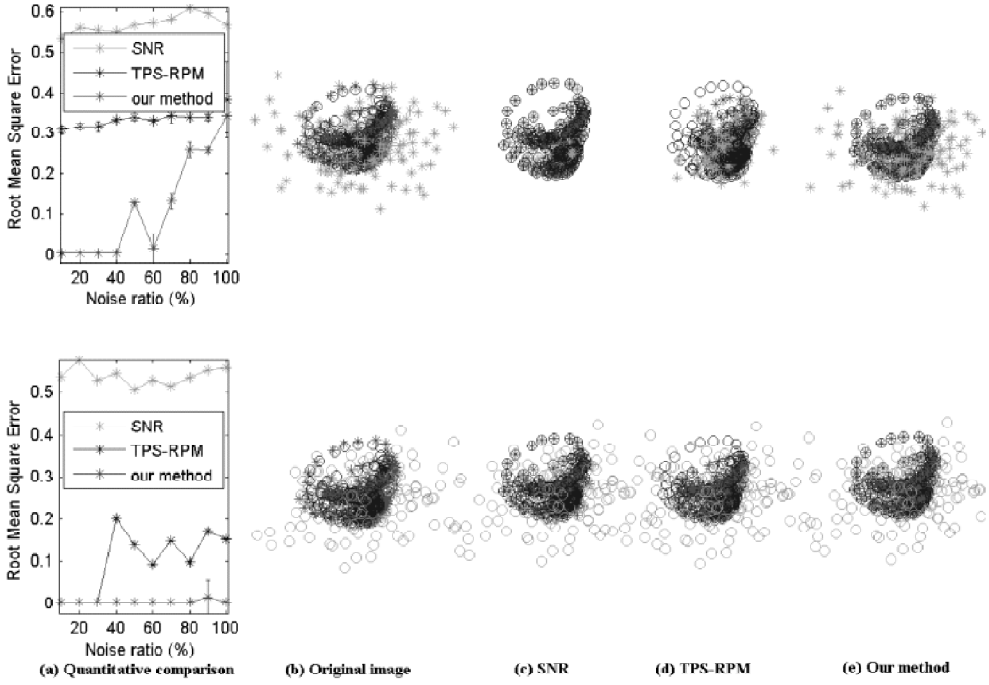

Figure 3: Performance comparison for noisy data set (top row) or noisy model set (bottom row). (a) RMSE curves; (b) to (e) The alignment of 3D face with 40% noisy data set (top row) and noisy model set (bottom row). Red stars are the points of original data set, and blue circles are the points of original model set. Green stars or circles are noise in data or model set, respectively. Ground truth is that all of the red starts are in an unique blue circle, but all of the green points are not mapped onto any points.

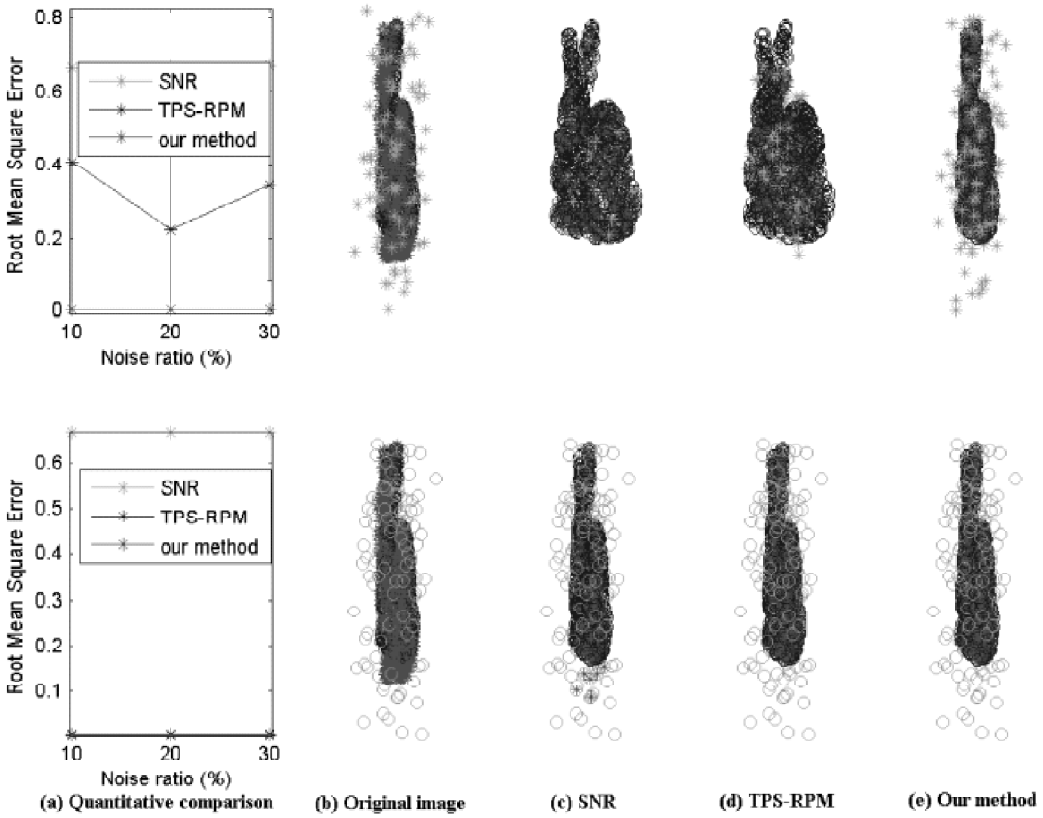

Figure 4: Performance comparison for noisy data set (top row) or noisy model set (bottom row). (a) RMSE curves; (b) to (e) The alignment of 3D bunny with 20% of noise ratio. Red stars are the points of original data set, and blue circles are the points of original model set. Green stars or circles are noise in data or model set, respectively. Ground truth is that all of the red starts are in an unique blue circle, but all of the green points are not mapped onto any points.

model set, 156 counterparts are wrong for 3D face when using SNR method. However, our method is able to easily find the noise and remove them with a combination of sparse error residuals and soft correspondence. Our method attains all right counterparts and therefore aligns two point sets well.

4.2. Results on incomplete datasets

Synthetic datasets were constructed as follows: the points of left face were proportionally deleted from data or model set; the points on head and ears of bunny were proportionally removed from data or model set. Three incomplete ratios were chosen: 10%, 20%, 30%.

Figure 5 demonstrates that our method performs better than the other methods on 3D face datasets. Since the face is entirely smooth, SNR always over-fits it with the sparsity of regularization. Both our method and TPS-RPM get the right correspondence when incomplete occurs in data set, but our method aligns more accurately than TPS-RPM. When some of model points are missing, the corresponding data points should not have the matched model points.

But TPS-RPM cannot find that. As a result, TPS-RPM transforms all data points onto the remained model points, and finally leads to a wrong alignment. With the sparsity error measurement, our method classified the inliers and outliers. Hence, matching results are closer to the ground truth when using our method.

Figure 6 also indicates that our method gives better registration results than the other methods for 3D bunny dataset. Since the head and two ears of bunny are removed, they should not have counterparts after registration. The results show that the removed points become the counterparts when using SNR. This is because the sparse regularization in SNR is set for the point sets with piecewise smooth, but the bunny is entirely smooth and thus over-fitting occurs. TPSRPM and our method yield similar results when the data set is incomplete, but our method attains better results than TPS-RPM

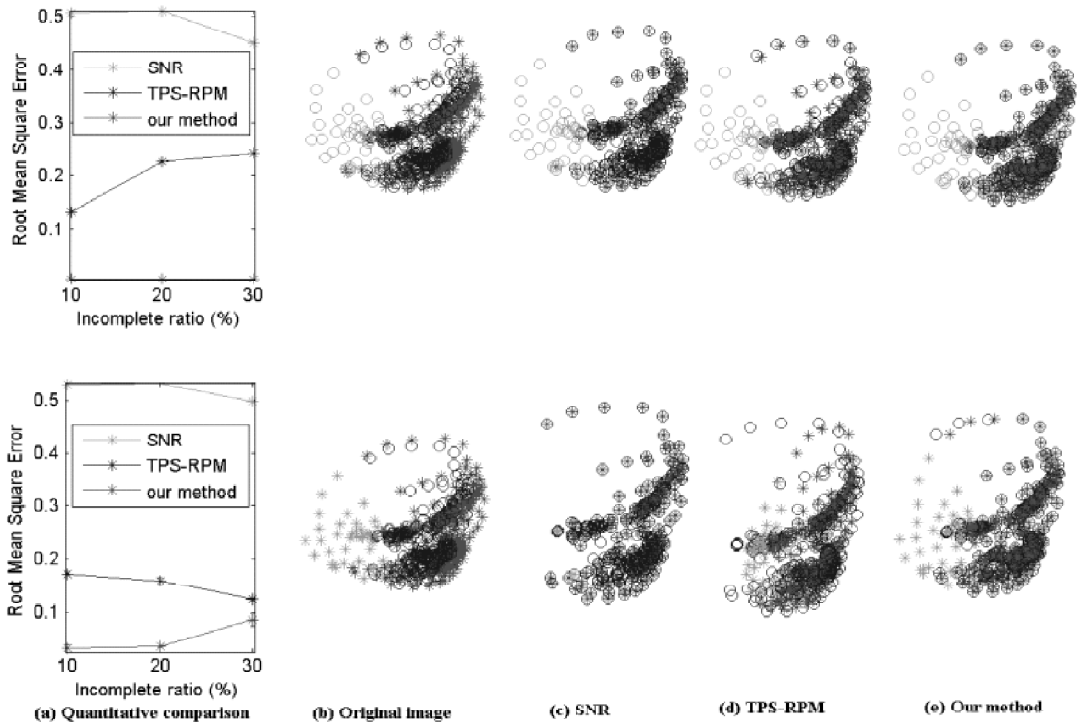

Figure 5: Performance comparison when data set (top row) or model set (bottom row) is incomplete. (a) RMSE curves; (b) to (e) The alignment of 3D face with 10% of incomplete ratio. The points in data or model set are labeled red and blue, respectively. The counterparts of removed points are labeled green. Ground truth is that all of the red and blue points are matched with each other, but all of the green points are not mapped onto any points.

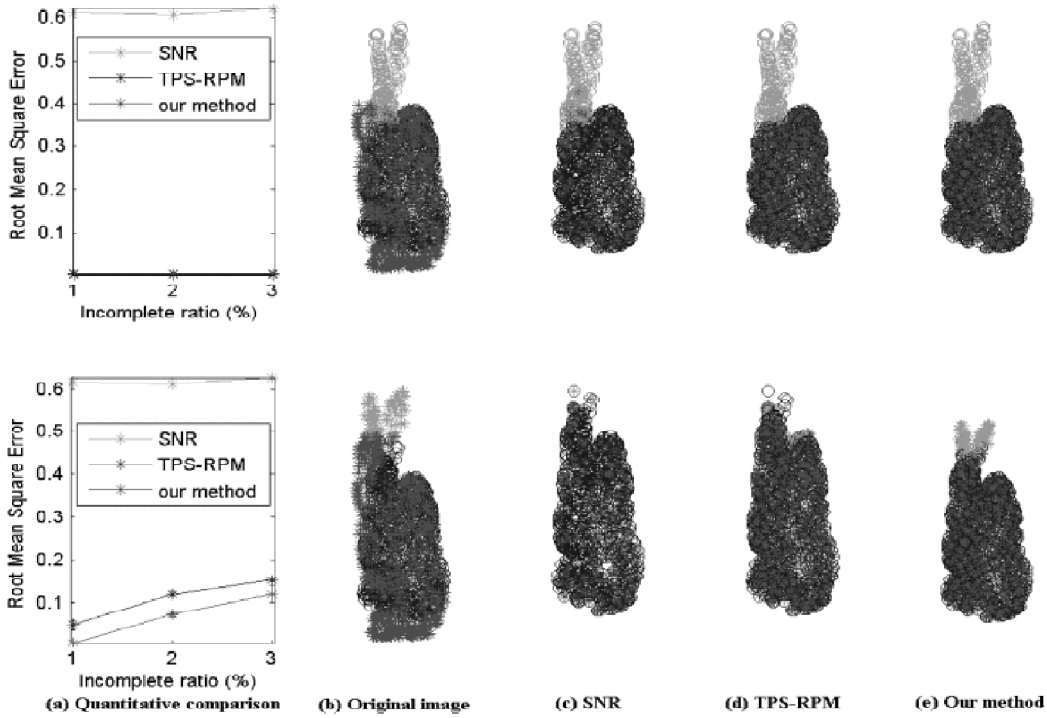

Figure 6: Performance comparison when data set (top row) or model set (bottom row) is incomplete. (a) RMSE curves; (b) to (e) The alignment of 3D bunny with 10% of incomplete ratio. The points in data or model set are labeled red and blue, respectively. The counterparts of removed points are labeled green. Ground truth is that all of the red and blue points are matched with each other, but all of the green points are not mapped onto any points.

when the model set is incomplete. The optimization is better in our method than in TPS-RPM, because the penalties of p-norms are smaller than that of the l_2 norm. As a result, the right counterparts were more easily detected using our method than the other methods.

4.3. Adaptive selecting of "p" values

The parameter p controls the performance of our method with respect to outliers. Its value is iteratively changed using Eqs. 14 and 15.

Figure 7 indicates that an adaptive p is more suitable than a fixed p when there are outliers. The value of p is fixed to 0.4, which is an empirical value used in Sparse ICP [19]. The value of p in p-norms is linked to the error residuals of outliers, but they cannot be known in advance. A fixed value of p can only handle the penalty associated with this value. The influence of outliers is gradually increased with a large value of p. On the other hand, the alignment will run much more slowly when using a much smaller value of p. In this paper, an adaptive value of p is applied. This value is dependent on error residuals. If a point has a larger error residual than other points, it is treated as an outlier and the value of p is decreased. Thus the penalty of this point is reduced and the alignment will not be skew. The intuitional results can be seen in Fig. 7.

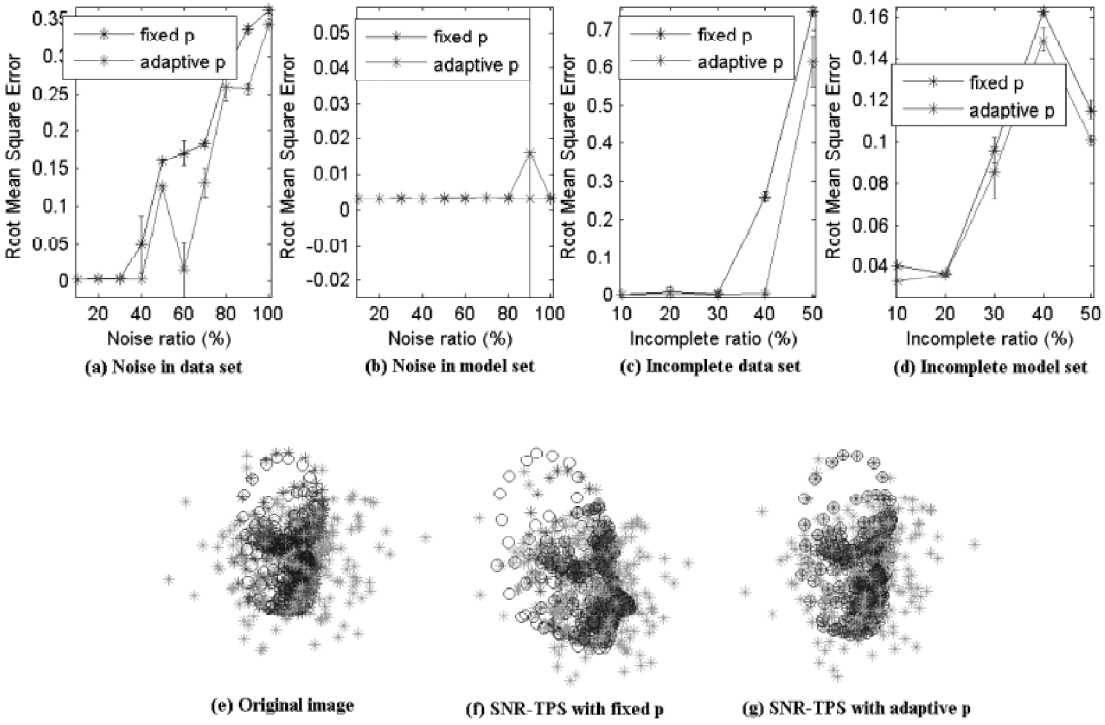

Figure 7: Performance comparison of a fixed p (p = 0.4) and an adaptive p. The top row shows the RMSE curves of different outliers. The bottom row gives an example when noise is present in data set and noise ratio is 40%. Red stars are the points of original data set. Blue circles are the points of original model set. Green stars are the noise in data set.

4.4. Convergence analysis

Convergence is an important element in the registration methods addressed in the present paper. For this reason, running time of different methods is first analyzed.

The above experiments were performed 10 times for all methods. Table 1 indicates that our method needs more time than TPS-RPM, but less time than SNR. The running time of our method is not dependent on the value of p. More points there are, more time all methods need.

Although with soft correspondence, TPS-RPM avoids the estimation of initial transformations and somewhat reduces the influence of outliers. But TPS-RPM cannot prevent local minimum (Fig. 8), even if it is in a deterministic annealing framework. That is because TPS-RPM cannot distinguish inliers and outliers. Soft corresponding point $\mathbf{c}_i$ will be wrong

Table 1: Comparison of computation time among the three methods (Unit: second)

Dataset	*Outliers*	*Methods*			
		TPS-RPM	*SNR*	*Fixed p*	*Adaptive p*
3D face	Noisy data set	14.4	1088.9	231.9	232.4
	Noisy model set	8.4	1137.7	79.5	81.9
	Incomplete data set	3.1	230.7	35.3	33.0
	Incomplete model set	5.3	707.7	82.6	86.4
3D bunny	Noisy data set	47.6	668.4	654.9	649.5
	Noisy model set	37.8	1137.7	420.7	418.4
	Incomplete data set	22.7	261.3	258.8	256.9
	Incomplete model set	31.1	325.8	420.8	417.9

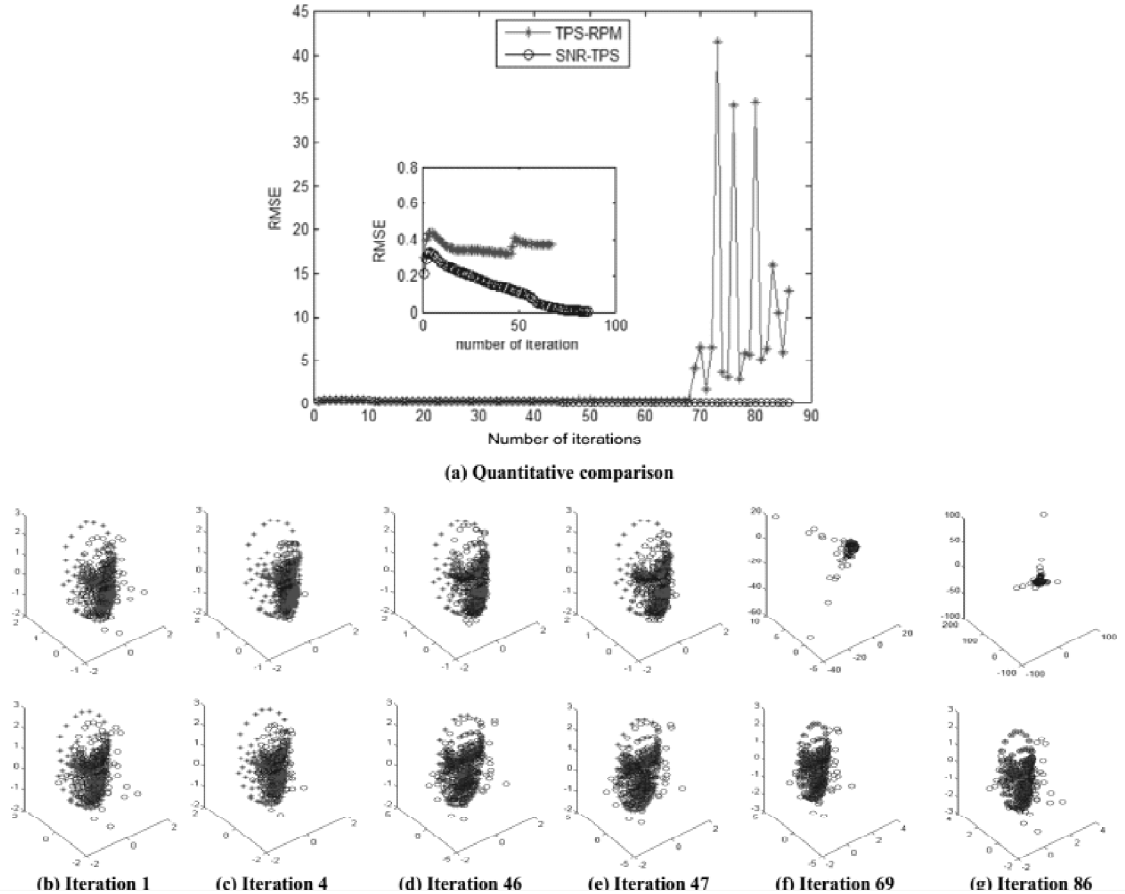

Figure 8: Convergence comparison of TPS-RPM (middle row) and our method (bottom row) when noise is in data set and noise ratio is 30%. Red stars are points in data set. Blue circles are points in model set.

for the point $\mathbf{x}_i$ when the outliers are close to $\mathbf{x}_i$. Then the optimization will be skew to punish the large error residual of the outliers.

In contrast to TPS-RPM, the error residual between $\mathbf{c}_i$ and $\mathbf{x}_i$ is sparse in our method. With the shrinkage operator [22], our method can detect whether the soft corresponding point $\mathbf{c}_i$ i is an outlier or inlier. If it is an outlier, it will be assigned a larger vector $\mathbf{e}_i$. Otherwise, it will remain unchanged. Therefore the new variable $\mathbf{e}_i$ is closer to its counterpart xi. Hence, our method will not fall into local minimum and produce more accurate results (Fig. 8).

Figure 9 shows that our method can find more accurate correspondences than the other methods. The number of correct correspondences found by our

method is much more than the other methods whether there is noisy point set or incomplete point set. That is because our method more easily distinguished the inliers and outliers with the sparse error residuals. So the alignment using our method is better than the other methods. Besides, more accurate counterparts are obtained when using adaptive p in comparison with the fixed p in most cases. Even if the number of counterparts is the same, smaller distance between the counterparts can be achieved when using adaptive p than when using fixed p in our method (Fig. 7).

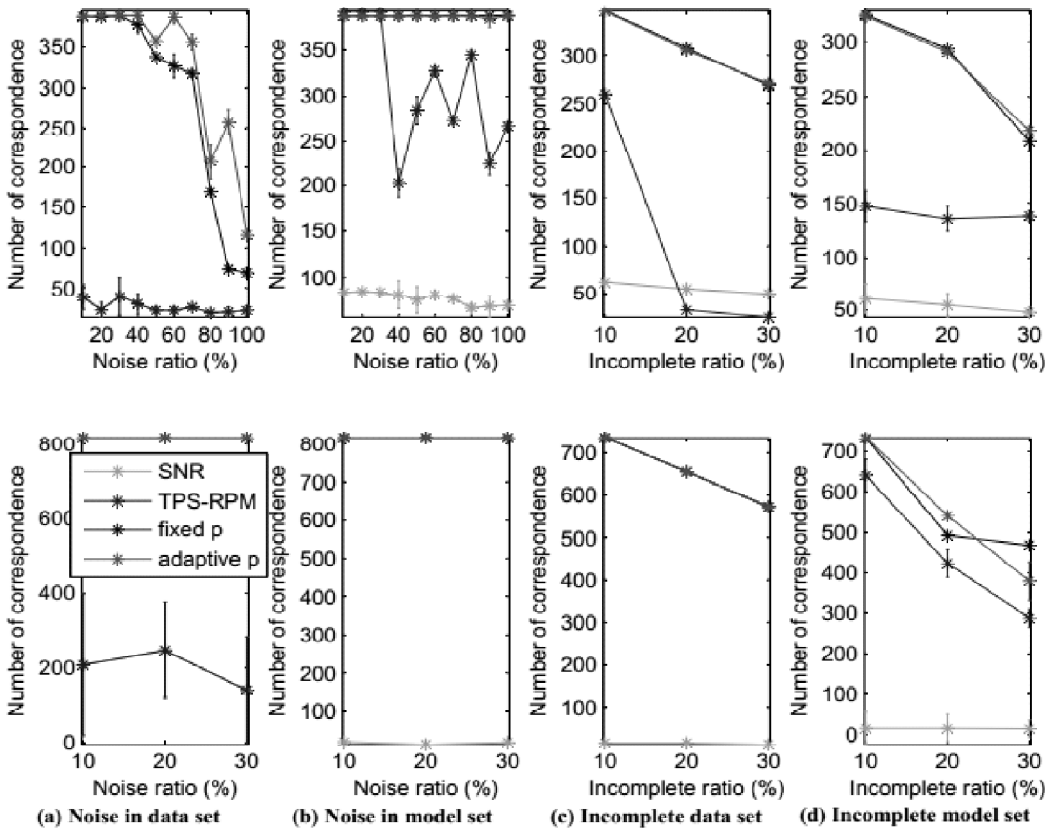

Figure 9: Correspondence comparison of three methods under four situations on 3D face (top row) and 3D bunny (bottom row).

4.5 Results on real datasets

In this section, the task is to automatically find the location of physiological points. The real data was from Shanghai 9th Hospital. The zygoma of the patient were constricted after operation. The ground truth of 13 physiological points were given empirically by a clinical doctor.

To evaluate the performance of our method, the pre-operation physiological points were mapped onto the postoperation face by the three methods. The RMSE values and matching results are shown in Fig. 10. TPS-RPM failed for all physiological points. The RMSEs of our method and SNR are 207 and 209, respectively. Due to the constriction of zygoma, the two temple points are the main failed points for our method and SNR. When removing them, the RMSEs of our method and SNR are decreased respectively to 55 and 57. With the use of ADMM, our method needs more time (2.9504s) than the other two methods (2.3627s for TPS-RPM and 0.1922 for SNR), but produces the results closer to the ground truth.

5. CONCLUSION

A sparse nonrigid registration based on TPS (SNR-TPS) is proposed for point sets. The method consists of introducing p-norms in TPS-RPM to reduce the penalty for large outliers, using a matching

probability matrix to achieve a soft correspondence, and combining deterministic annealing and Alternating Direction Method of Multipliers (ADMM) to optimize TPS-based nonrigid transformations. The results show that the proposed method performs better than

TPS-RPM and SNR when outliers are present in the point sets.

In the future, we will improve the efficiency of the proposed method (SNR-TPS) using a combination of approximate distance queries, subsampling and parallel execution. On the other hand, how to effectively use sparsity on both of error residuals term and regularization term is an interesting future work.

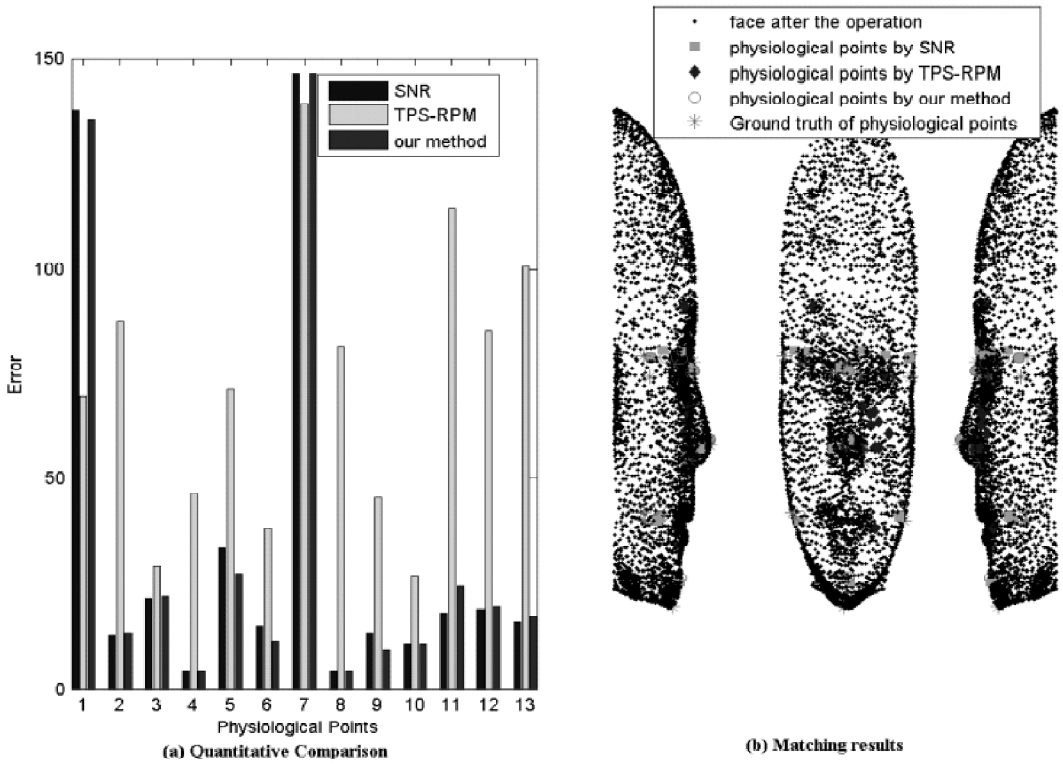

Figure 10: Performance comparisons with respect to the physiological points. (a) quantitative comparison; (b) matching results.

ACKNOWLEDGMENTS

This research is partly supported by NSFC, China (No: 31100672), NSFC, China (No: 61375048), NSFC, China (No: 61802247) and Committee of Science and technology, Shanghai (No:11530700200).

REFERENCES

1. H. Chui and A. Rangarajan, "A new algorithm for non-rigid point matching," in Computer Vision and Pattern Recognition, 2000. Proceedings. IEEE Conference on, 2, 44–51, IEEE (2000).
2. H. Chui and A. Rangarajan, "A new point matching algorithm for non-rigid registration," Computer Vision and Image Understanding 89(2), 114–141 (2003).
3. P. J. Besl and N. D. McKay, "A method for registration of 3-d shapes," IEEE Transactions on pattern analysis and machine intelligence 14(2), 239–256 (1992).
4. M. A. Fischler and R. C. Bolles, "Random sample consensus: a paradigm for model fitting with applications to image analysis and automated cartography," Communications of the ACM 24(6), 381–395 (1981).
5. A. Hast, J. Nysjo, and A. Marchetti, "Optimal ransac-towards a repeatable algorithm for finding the optimal set," Journal of Wscg 21(1), 21–30 (2013).
6. O. Chum, J. Matas, and J. Kittler, "Locally optimized ransac," Lecture Notes in Computer Science 2781, 236–243 (2003).

7. O. Chum, J. Matas, and S. Obdrzalek, "Enhancing ransac by generalized model optimization," in Proc. of the ACCV, 2, 812–817 (2004).
8. K. Lebeda, J. Matas, and O. Chum, "Fixing the locally optimized ransac–full experimental evaluation," in British Machine Vision Conference, 1–11, Citeseer (2012).
9. A. Myronenko, X. Song, and M. A. Carreira-Perpinan, "Non-rigid point set registration: Coherent point drift," Advances in Neural Information Processing Systems 32(12), 1009–1016 (2006).
10. A. Myronenko and X. Song, "Point set registration: Coherent point drift," IEEE Transactions on Pattern Analysis and Machine Intelligence 32(12), 2262–2275 (2010).
11. P. Wang, P. Wang, Z. Qu, Y. Gao, and Z. Shen, "A refined coherent point drift (cpd) algorithm for point set registration," Science China Information Sciences 54(12), 2639–2646 (2011).
12. Q. Sang, J. Zhang, and Z. Yu, "Non-rigid point set registration: a bidirectional approach," in Acoustics, Speech and Signal Processing (ICASSP), IEEE International Conference on, 693–696, IEEE (2012).
13. Y. Gao, J. Ma, J. Zhao, J. Tian, and D. Zhang, "A robust and outlier-adaptive method for non-rigid point registration," Pattern Analysis and Applications 17(2), 379–388 (2014).
14. G. K. Tam, Z.-Q. Cheng, Y.-K. Lai, F. C. Langbein, Y. Liu, D. Marshall, R. R. Martin, X.-F. Sun, and P. L. Rosin, "Registration of 3d point clouds and meshes: a survey from rigid to nonrigid," Visualization and Computer Graphics, IEEE Transactions on 19(7), 1199–1217 (2013).
15. H. Hontani, T. Matsuno, and Y. Sawada, "Robust nonrigid icp using outlier-sparsity regularization," in Computer Vision and Pattern Recognition (CVPR), 2012 IEEE Conference on, 174–181, IEEE (2012).
16. Y. Yu, S. Zhang, K. Li, D. Metaxas, and L. Axel, "Deformable models with sparsity constraints for cardiac motion analysis," Medical image analysis 18(6), 927–937 (2014).
17. J. Yang, K. Li, K. Li, and Y.-K. Lai, "Sparse non-rigid registration of 3d shapes," in Computer Graphics Forum, 34(5), 89–99 (2015).
18. R. Chartrand, "Exact reconstruction of sparse signals via nonconvex minimization," Signal Processing Letters, IEEE 14(10), 707–710 (2007).
19. S. Bouaziz, A. Tagliasacchi, and M. Pauly, "Sparse iterative closest point," in Computer graphics forum, 32(5), 113–123 (2013).
20. P. Mavridis, A. Andreadis, and G. Papaioannou, "Efficient sparse icp," Computer Aided Geometric Design 35, 16–26 (2015).
21. R. Chartrand and B. Wohlberg, "A nonconvex admm algorithm for group sparsity with sparse groups," in Acoustics, Speech and Signal Processing (ICASSP), 2013 IEEE International Conference on, 6009–6013, IEEE (2013).
22. G. Marjanovic and V. Solo, "On optimization and matrix completion," Signal Processing, IEEE Transactions on 60(11), 5714–5724 (2012).